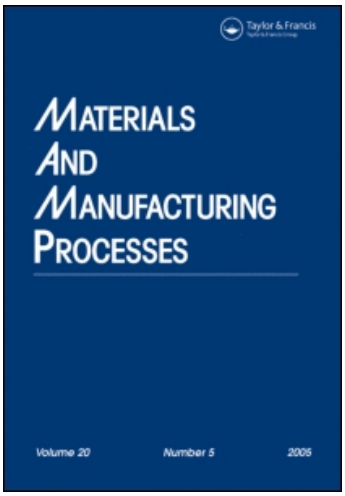

Materials and Manufacturing Processes
Publication details, including instructions for authors and subscription information:
http://www.informaworld.com/smpp/title~content=t713597284

Effect of Carbide Precipitation on the Structure and Hardness in the Heat-Affected Zone of Hadfield Steel After Post-Cooling Treatments

E. Curiel-Reyna [a]; J. Contreras [a]; T. Rangel-Ortis [a]; A. Herrera [ab]; L. Baños [c]; A. del. Real [b]; M. E. Rodríguez [b]
[a] Centro de Asimilación Technológica, FES-Cuautitlán, Universidad Nacional Autónoma de México, Cuautitlán-Izcalli s/n, Edo. de México [b] Centro de Física Aplicada y Tecnología Avanzada, Universidad Nacional Autónoma de México, Juriquilla s/n, Juriquilla, Querétaro, Qro. Mexico [c] Instituto de Investigación en Materiales, UNAM, Ciudad Universitaria, México D.F, México

Online Publication Date: 01 January 2008

To cite this Article Curiel-Reyna, E., Contreras, J., Rangel-Ortis, T., Herrera, A., Baños, L., Real, A. del. and Rodríguez, M. E.(2008)'Effect of Carbide Precipitation on the Structure and Hardness in the Heat-Affected Zone of Hadfield Steel After Post-Cooling Treatments',Materials and Manufacturing Processes,23:1,14 — 20
To link to this Article: DOI: 10.1080/10426910701524352
URL: http://dx.doi.org/10.1080/10426910701524352

Materials and Manufacturing Processes, 23: 14–20, 2008

ISSN: 1042-6914 print/1532-2475 online
DOI: 10.1080/10426910701524352

Taylor & Francis
Taylor & Francis Group

Effect of Carbide Precipitation on the Structure and Hardness in the Heat-Affected Zone of Hadfield Steel After Post-Cooling Treatments

E. Curiel-Reyna[1], J. Contreras[1], T. Rangel-Ortis[1], A. Herrera[1,2], L. Baños[3], A. del. Real[2], and M. E. Rodríguez[2]

[1]*Centro de Asimilación Technológica, FES-Cuautitlán, Universidad Nacional Autónoma de México, Cuautitlán-Izcalli s/n, Edo. de México*
[2]*Centro de Física Aplicada y Tecnología Avanzada, Universidad Nacional Autónoma de México, Juriquilla s/n, Juriquilla, Querétaro, Qro. Mexico*
[3]*Instituto de Investigación en Materiales, UNAM, Ciudad Universitaria, México D.F., México*

The aim of this work was to investigate the effect of the carbides precipitated on the hardness and structure in the heat-affected zone of a Hadfield steel that has been used as broke stone tool during ten months and that have to be repaired by the welding process. The steel presents significant structural changes for the presence of the discontinuities in the heat-affected zone, that affect the hardness and the structure in comparison to the homogenized sample. The investigation is carried out with X-ray diffraction (XRD), microhardness Vickers, and Scanning Electron Microscopy (SEM) system. According to the XRD patters, the presence of Manganese carbides was identified. The identification of the types of carbides present in the steel structure allows us to say that it belongs to the $Mn_{23}C_6$ and Mn_7C_3 type.

Keywords Austenite; Carbides precipitate; Cooling rate; Grain; Grain boundary; Hadfield steel; Hardness; Heat-affected zone; High carbon; High manganese; Homogenized; Microfissures; Microhardness; Precooling; Structural properties.

Introduction

Hadfield steel (austenitic steel with high Mn 10 to 14 wt%, and high C: 1 to 1.4 wt% content) is routinely used in heavy industrial components such as mill hammers, oil derrick, railroading, and cement manufacturing among others; for both high impact resistance (at room and low temperatures) and high superficial wear resistance, including metal–metal friction. Indeed, the austenite stability and its excellent transition temperature, along with its ability to harden with work, make these alloys popular for the mining industry, chemical grinding, high wear-and-tear processes; however their chemical composition makes Hadfield alloys difficult to repair by welding, thus limiting their industrial applications [1].

Practically, no attention has been paid to the failure of Mn steels because its austenitic matrix is considered sufficient guarantee of high impact toughness. However, steel of the type with a single-phase austenitic structure is seldom used under high wear-and-tear conditions. The specific chemical composition of Hadfield steel indicates up to 1.5% C, a large quantity of carbides form impairing the impact toughness [2].

The presence of carbides in grain boundary or in the grain has an adverse influence on the tenacity; small quantities of carbides decrease the energy to fracture toughness considerably in the austenitic manganese steel. The absence of carbides is related with the chemical composition, heat treatment, and piece size [3].

Successful welding or hard surfacing of these castings depends on the properties of the heat-affected zone. In unalloyed Hadfield steel, the zone is susceptible to cracking due to the volume changes during the precipitation of transformation products upon reheating. The transformation products are carbides and pearlite [4].

Recently, Curiel et al. [5] studied the evolution of defects, particularly voids, microvoids, carbide precipitates, and microfractures caused by the cooling rates on the heat-affected zone. According to their results, the homogenized samples exhibited residual stress and lower crystalline quality. The results indicate that if the cooling rate decreases, the crystalline quality, grain hardness, and grain microhardness increases. The sample cooled in oil showed changes in void formation when compared to the homogenized sample. In the case of air cooling, there were increments in void sizes, microfissures, and carbide precipitation. Finally, for the furnace-cooled sample, the presence of microfissures and fractures was evident, and a significant carbide precipitation exhibiting different morphology was observed [5].

Chernat et al. [6] studied the influence of the carbon and manganese contents and different hardening treatments on the structure and properties of high manganese steels in order to establish the influence of thermomechanical and thermocyclic treatment on the mechanical properties of steel. The results showed that the hardenability of unstable

Received December 27, 2006; Accepted March 19, 2007

Address correspondence to M. E. Rodríguez and E. Curiel-Reyna, Centro de Física Aplicada y Tecnología Avanzada, Campus Juriquilla, Universidad Autónoma de México, A. P. 1-1010, Querétaro, Qro, México; E-mail: marioga@fata.unam.mx

steel based on manganese austenite is higher than the one presented in relatively stable steel, it means having high hardenability during thermomechanical treatment, good resistance level that influenced the failure, impact, hydroabrasive wear, and fatigue resistance [6].

Ductile failure of steels can be divided into three stages: void nucleation, void growth, and void coalescence. There are many criteria to describe the process of void nucleation. Some give a critical stress, others use a critical strain. Both types of criteria are based on the fact that a critical stress at the interface of an inclusion causes detachment or cracking on the particle. The process of void growth presupposes a plastic deformation of the matrix. The increase of the void volume strongly depends on the state of stress. The ductile failure is the coalescence of voids representing the initiation of a microcrack. There are several micromechanisms as well as several criteria to describe coalescence [7].

The foregoing investigations were related to the study of nonmechanical worked Hadfield steel. The objective of this work is to present the study of the main phases presented in the heat-affected zone of worked Hadfield steel after welding.

Methods and materials

Sample Description

The steel under investigation belonged to the high manganese net alloyed type whose chemical composition is: 1.16% C, 12% Mn, 0.46% Si, 0.04% P, 0.03% S, 0.1% Cr, 0.1% Mo, and 0.15% Ni. In this case Cr, Mo, and Ni were residual elements, coming from the commercial melting process. The other elements were found in the range of the American Society Testing of Materials (ASTM) standard. The chemical composition of the electrode (AWS A5.13) that was used for welding is: 0.72% C, 12.53% Mn, 3.89% Ni, 0.25% Cr, 0.94% Si, 0.02% P, and 0.02% S.

Preparation of the Samples

Eight samples of 115 × 19 × 3 mm were used for this study. Initially each sample was heated to 1100°C during 45 min. All the samples were previously packed using graphite powder in order to avoid possible decarburation. These samples were quenched in water to obtain a homogeneous structure of austenite as was reported before [9, 10]. One sample was taken as a reference, and the other samples were welded and cooled under different thermal conditions. The welding process was carried out as follows: Two parts were put in contact and then a welded bead was placed between them, as it is shown in Fig. 1(a). The final samples were obtained under the following cooling conditions: A bead welding was made using electrodes of 4.0 mm of diameter in the center of the samples. The welding was done using a Shield Metal Arc Welding (SMAW) process with a Hobart 300. An E-FeMn-A electrode type was used according to the standard American Welding Society (AWS) employing a current of 138 amperes. After this process, the sample thickness at the central part was reduced to 16 mm by electro erosion

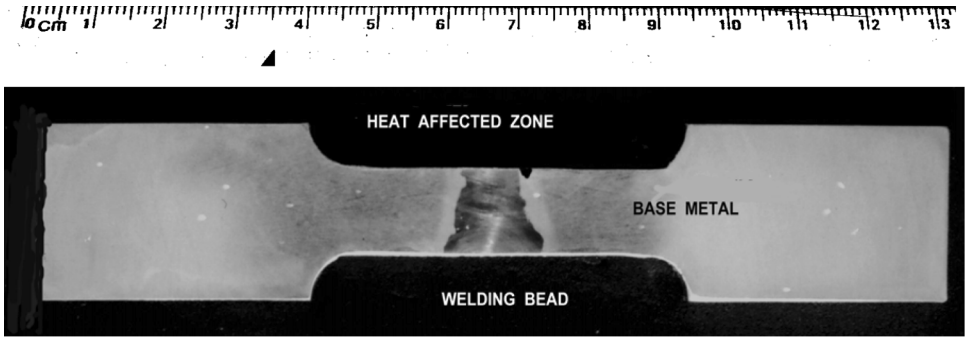

(a)

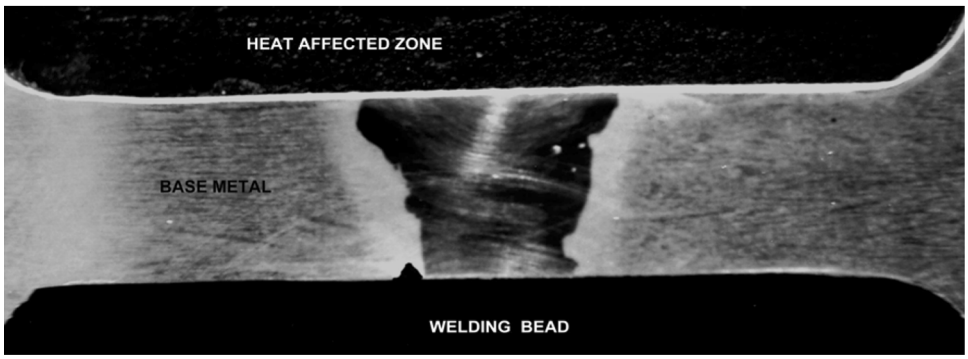

(b)

Figure 1.—(a) and (b) show the samples used for tension test and the heat-affected zone.

technique. Next to the heat-affected zone, on one side of the sample, a notch 2 mm deep (v shape) was made in order to induce the fracture in the heat-affected zone [Fig. 1(b)]. The structural changes in the heat-affected zone of these samples were studied by metallographic analysis, XRD, and microhardness measurement in Vickers.

Metallographic Analysis

The metallographic analyses of the polished samples were performed using a Scanning Electron Microscopy (SEM) system, Philips XL-30 at high vacuum (1 to 5 torr).

XRD

The XRD patterns were taken using a Siemmens Crystaloflex 5000 operating at 35 kV, 15 mA with Cu K_{α} line. The experimental data to determine the presence of crystalline phases was analyzed by a Dataflex program. All the studied samples, including the references, were cut off from the center.

Microhardness Measurements

The Vickers scale was used to measure the microhardness of the polished samples. The reported value is an average of 30 measurements across the surface of the sample, using the Wilson microhardness tester with a Vickers diamond penetrator and a Zeiss optic microscope. The microhardness was determined in the Austenite grain and the grain boundary.

Results and discussions

Figures 2(a), (b) show the SEM images of microstructure from blank reference sample, taken at 2000X and 200X magnifications, respectively. The presence of small amounts of micro-voids (from 1 to 3 μm) aligned across the surface in the grains boundaries was noticed. The incidence of carbides in the grain boundary or Austenite grain in the pictures was not identified.

Figures 3(a), (b) show the SEM images of the sample surface in the heat-affected zone, furnace treatment at 300°C for 60 minutes from the cooling air condition. Figure 3(a) shows at 2300X a noticeable precipitation of carbide of differences forms in grain boundary, the average size of this precipitate is between 3 and 10 μm. In Fig. 3(b), at 2500X, the presence of massive intergrain carbide was recognized. Also it is important to notice the existence of needles form carbide in the bulk and the austenite grains. The presence of

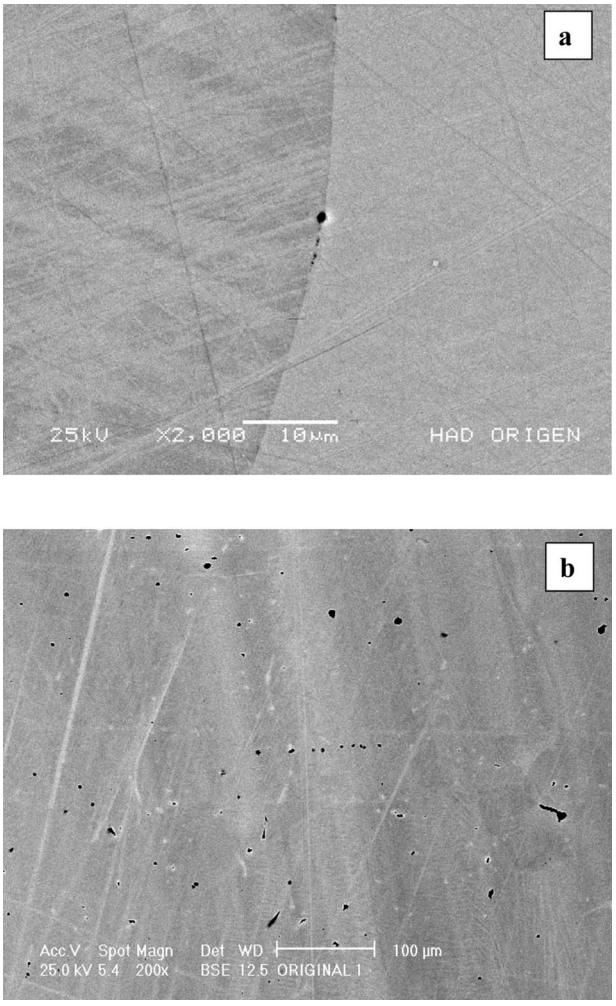

FIGURE 2.—(a) and (b) show SEM images of the homogenized sample, showing the existence of holes and grains boundaries.

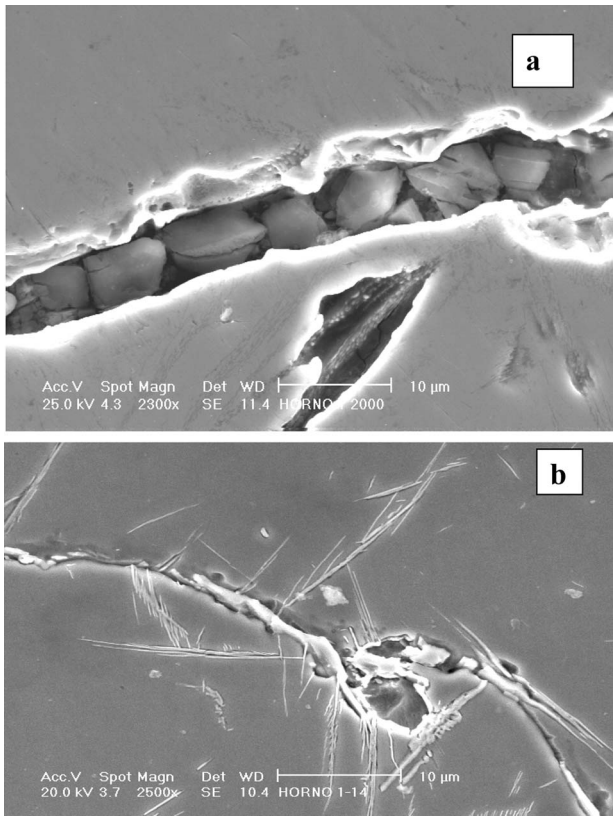

FIGURE 3.—(a) and (b) shoe the sample cooled in furnace at 300°C, fractures with carbides and continuous carbides in grain boundary regions.

inter-grains carbides has also been reported [12, 13], stating that it directly depends on the chemical composition of the steel and the cooling rate. However, the phase identification of this precipitate has been not reported. The localization of the carbides precipitate is present into the fracture or also can be associated with the initial fracture process in this kind of steel [5]. If we compare Figs. 3(a), (b) it is clear the presence of precipitate in the heat-affected zone has two different ways: the first one exhibits micro-precipitate formations [Fig. 3(a)] and in the second case the precipitate located into the fracture exhibit a continuous way. This fact could affect the carbide precipitate structure, because this precipitate can be present as M_7C_3 and $M_{23}C_6$.

Figures 4(a), (b) show the SEM image using back scattering electrons on the surface of the HAZ from the sample with seams weld cooled with air. In Fig. 4(a) at 800X, the presence of particles of micro-carbides along the grain boundary way is observed; the fissures were identified as micro-carbide that could also appear in the bulk region outside the fissure regions. In Fig. 4(b) at 4000X [region A in Fig. 4(a)], it is possible to identify the presence of massive intergrain carbide similar to islands, but in this case it is possible to associate its existence to the fissure region. It is clear that after the heat treatment there exist two different carbide formations in size and also it is necessary to explore its structural composition. This fact also can influence the mechanical properties of this material in the heat affected zone.

Figures 5(a), (b) show the SEM images of the sample quenched in oil at 17°C. Figure 5(a) taken at 250X, shows the existence of isolated carbides also small voids in the grain boundary can be observed. In Fig. 5(b) taken at 5000X, it is possible to identify the existence of small carbides and great massive carbide inside void. It is clear that in this case, in the region close to the heat-affected zone the boundary grain is isolated by micro-voids, the carbide region in the case of samples quenched in oil is smaller than the carbide formation in sample quenched in air.

It is clear according to Figs. 3, 4, and 5 that the carbides precipitate exhibits different ways and sizes; in the next

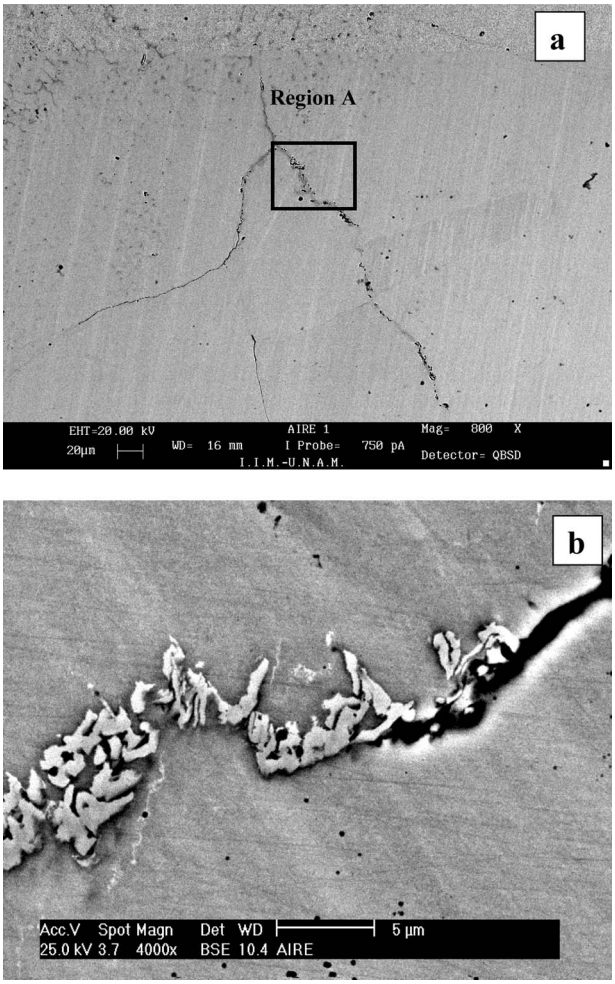

FIGURE 4.—(a) and (b) show the sample cooled in air quite. Region A in (b) shows grain boundary and (b) shows the existence of carbides associated with a fissure.

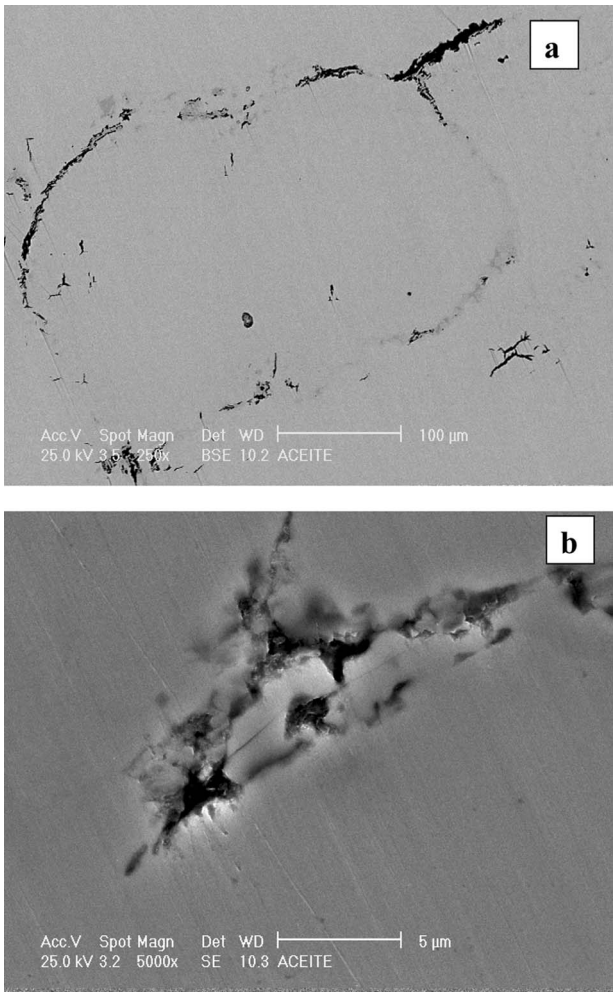

FIGURE 5.—(a) and (b) show the SEM images of sample quenched in oil with the presence of grain boundaries and fissures and (b) shows the carbide in grain boundary associated with voids.

section we will explore the structural configuration of this precipitate.

The XRD patters were obtained in the heat-affected zone using samples of $15 \times 15 \times 3$ mm to determine the structural configuration of the steel and carbide precipitate as a function of the cooling treatment. Figure 6(a) shows the XRD patters of the high Manganese steel and high Carbon under weld and non-welding conditions cooled in furnace, air, oil, and homogenized samples. The final conditions that were obtained in the heat-affected zone structure of the Hadfield steel after the welding and post-cooling treatments, compared to the structure of the wear original sample homogenized at 1100°C during 60 minutes, showed that some significant differences exist in the austenitic structure of the steel. In order to study the structural changes in the heat-affected zone as result of the treatment, it is necessary to study each one of the peaks found in the XRD pattern.

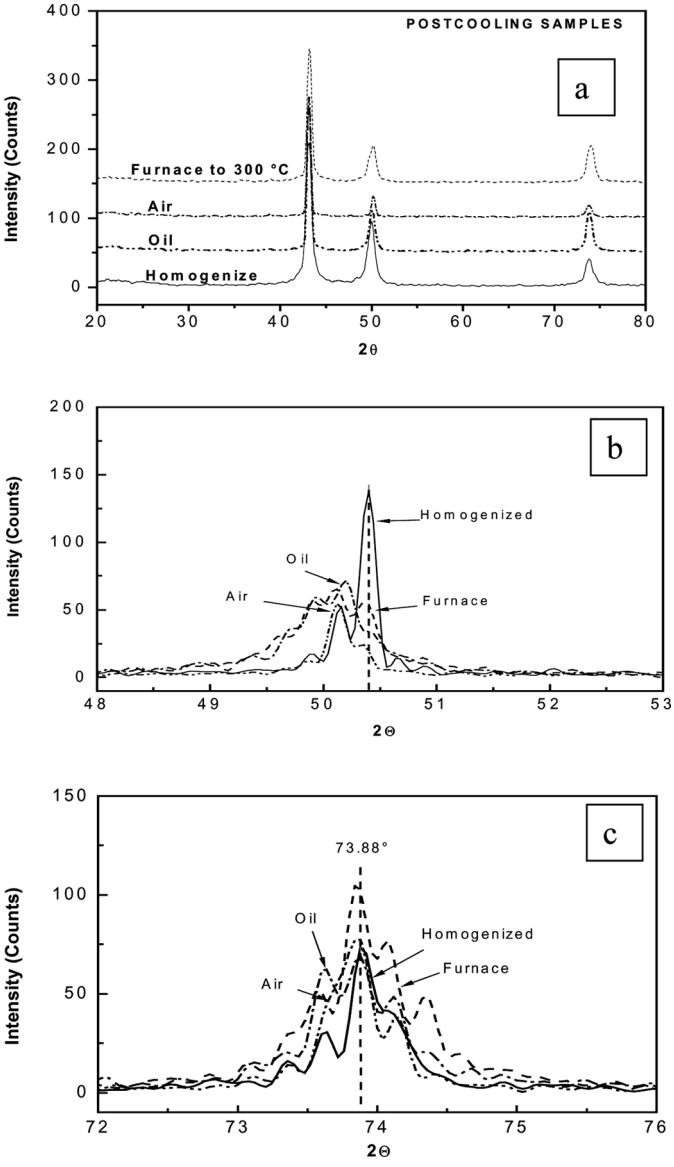

FIGURE 6.—XRD patters for three characteristics peak of Hadfield steel on the heat affected zone (a) and the peak located around 51°in 2Θ scale (b) and the peak located around 74° also used to phase identification.

Figures 6(b), (c) show the second and third peaks located at 50° and 74° of 2θ scale from Fig. 6(a) of the samples that were treated with post-cooling treatments after being welded, compared with the wear original sample that was homogenized, in which the differences among the 4 curves of the XRD are observed. According to these figures there exist different crystalline structures associated in the heat-affected zone as a result of the cooling processes. The results obtained in the Austenite structure and the phases were determined by the investigation of the XRD data and the ternary phase diagram of Fe–Mn–C [8]. According to this data, there is an agreement between the crystalline structure obtained for homogenized sample and the ternary diagram and the chemical composition of the steel Hadfield under investigation which contain 1.16 wt% C, 12 wt% Mn. However after a detailed analysis of the peaks showed in Figs. 6(b), (c), there are other structures associated to these peaks that have to be identified.

Table 1 shows the results of the interatomic distances calculated from peaks showed in Figs. 6(b), (c) using Bragg's law, $n\lambda = 2d \sin\theta$ and DIFRAC-AT program [11]. Comparing the inter-atomic distances obtained for each one of the peaks found in these figures, with the XRD tables, it is possible to have the phase identification.

The phase diagram of Fe–Mn–C in equilibrium establishes the formation of the following phases: Austenite, Mn_3C, and Mn_7C_3, but by carefully studying the interplanar

TABLE 1.—Interplanar distance of samples and the structural identification of phases present in the heat-affected zone.

Samples	Peak 2°	Peak 3°
Homogenize	1.828 Å	1.291 Å
	1.819 Å	1.286 Å
	1.811 Å	1.283 Å
Furnace to 300°C	1.836 Å	1.288 Å
	1.827 Å	1.283 Å
	1.820 Å	1.280 Å
Air	1.828 Å	1.291 Å
	1.820 Å	1.283 Å
	1.810 Å	1.279 Å
Oil	1.834 Å	1.286 Å
	1.825 Å	1.283 Å
	1.817 Å	1.278 Å
Structures		
Fe γ	1.8086 Å	1.2789 Å
	(200)	(220)
	80%	50%
M_3C	1.8543 Å	1.2253 Å
	(221)	(401)
	43%	14%
M_7C_3	1.8396 Å	1.2927 Å
	(301)	(051)
	100%	–
$M_{23}C_6$	1.7890 Å	1.2840 Å
	(531)	(820)
	20%	5%

distance for peaks showed in these figures, it was possible to identify by simultaneous analysis of both peaks the crystalline phases present in the material. Austenite (200) and (220), and Mn_7C_3 (301) and (051) were found in both peaks, but there exists other peak that is not in agreement with the usual phases for this material. Calculating the interplanar distance corresponding to these peaks and correlating them to the XRD data [11] and the peak intensity, this peak was identified as $M_{23}C_6$ (531) and (820). The important feature in the XRD patterns is that the presence of $M_{23}C_6$ does not correspond to the equilibrium phases of carbides in Hadfield steel.

The physical explanation of this fact can be as follow: It is well known that during the homogenized process in Hadfield steel under no working conditions does it have any kind of carbide precipitate. However, in the same homogenized process but in working steel, it exhibits the carbide formation that can be detected through the XRD but there is no evidence of its presence using SEM analysis. Due to the strong heat flux during the welding process in the heat-affected zone, there exists a carbide out-diffusion that can produce complex carbide phases. In the samples of the tension test corresponding to the procedures of post-cooling welding, as well as to the sample considered as original wear, 30 microhardness readings in grain boundary and grain austenitic bulk in the heat-affected zone were taken. The result of the average of the 30 readings of each sample is presented in Fig. 7. The violent entry and exit of heat for the electric arch of the welding process in the heat-affected zone of the Hadfield steel generates the energy retention that causes stress and a tendency of the structure to fracture, as well as the carbides precipitation. The measurement of the microhardness of the samples post-cooling welded, in grain boundary and mass of the grains of Austenite next to the fusion line in the heat-affected zone presented a significant difference against the hardness of the homogenized sample. Due to the precipitation of carbides in the grain boundary and in the mass of the grains of Austenite, during the continuous treatments of cooling, the hardness of the material was increased, besides the presence of cracks, fissures, and microfissures(5).

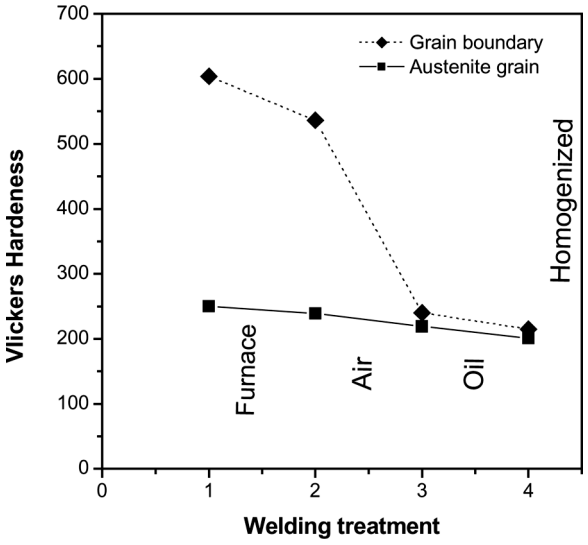

FIGURE 7.—Vickers microhardness of grain and grain boundary of samples in the heat-affected zone.

CONCLUSIONS

- The experimental conditions of the cooling rate treatments postwelding in the welding procedures had a considerable effect in the hardness of the structure of the material mainly caused by the presence of hard phases (precipitation of carbides) due to the permanency of heat in the Hadfield steel mass through the cooling speed.
- Homogenization treatment is recommended at high temperatures in order to avoid the presence of hard phases in the structure of the steel. However, the XRD of the homogenized sample showed in the 3° peak the presence of Manganese carbides. The identification of the types of carbides present in the steel structure allows to say that it belongs to the type $Mn_{23}C_6$ and Mn_7C_3, although a homogenization treatment states the opposite [10].
- The carbides of Manganese present a very high stability, in spite of the high temperature of the welding arc.

ACKNOWLEDGMENTS

This work was supported by project PAPIIT 13606, UNAM, 2006. The authors want to thank M. en I. Maria de Los Angeles Cornejo and Q. Carmen Vazquez for the technical support of this work.

REFERENCES

1. Cubberly, W.H. Wear resistant materials. Metals Handbook ASM. Austenitic Manganese Steel. 9a Ed.; 1980; Vol. 3, 568–588.
2. Bertold, V. Effect of structure of manganese steel on its mode of failure. Microstructure and mechanical properties of aging material, Ed. by Liaw, P.K., Vishwanathan, R., Murly, K.L., Simonen, E.P., Frear, D. The Minerals, Metals and Materials Society **1993**, 461–465.
3. Maratray, F. Nuevas tendencias para la mejora de los aceros austeníticos al manganeso. Colada, Revista Técnica de Fundición-España, **1979**, (12), 1–10.
4. Borik, F.; Scholz, W.G. Effects of time and temperature on ductility and toughness of modified austenitic manganese steels. AFS Transcactions 1971; 110–115.
5. Curiel-Reyna, E.; Herrera, A.; Castaño, V.M.; Rodríguez, M.E. Influence of cooling rate in the structure of heat-affected zone after welding a high manganese steel. Materials and Manufacturing Processes **2005**, *20*, 813–822.
6. Chernyak, S.S.; Levin, B.M.; Ivakin, V.L. Structure and properties of unstable austenitic high manganese steels. Izvestiya VUZ Chernaya Metallurgiya **1987**, 77–81.
7. Arndt, J.; Dahl, W. Effect of void growth and shape on the initiation of ductile failure of steels. Computational Materials Science **1997**, *9*, 1–6.
8. Roberts, G.A.; Cary, R.A. Tool Steels, **1980**, 4th Edition, American Society for Metals, Metals Park, Ohio 44073, USA, pp. 188–190.
9. ASM Committee on Austenitic Manganese Steels, Howard S. Avery, Douglas V. Doane and Herman A. Fabert Jr. American

Society for Metals, **1992**. Metal Handbook ASM, 9a. Edition, USA; Vol. 9, 568–588.
10. Welding Handbook AWS; American Welding Society USA; **1984**, 7a. Edition; 4° Vol., 195–209.
11. Powder Diffraction File, ASTM International Center Diffraction Data (ICDD); The Join Committee of Ponder Diffraction Standards 2004.
12. Curiel-Reyna, E.; Herrera, A.; Castaño, V.; Rodríguez, M.E. Influences of the precooling treatment in the heat affected zone of the welding in used Hadfield-type steel. Material and Manufacturing Processes **2006**, *21*, 562–567.
13. Kerlins, V.; Phillips, A. Metal Handbook ASM. Fractography, 9th ed.; 1980; Vol. 1, Chapter Modes of Fracture, pp. 18–20.